Evaluating HIV-1 Infectivity and Virion Maturation Across Varied Producer Cells with a Novel FRET-Based Detection and Quantification Assay

Aidan McGraw[1†], Jeongpill Choi[1†], Kedhar Narayan[1†], Shreyas S. Gujar[1], Caroline N. Arnette[1], Hasset Tibebe[1], Lilia Mei Bose[1], Grace Hillmer[1], Cailyn Sullivan[1], Taisuke Izumi[1, 2*]

[1]Department of Biology, College of Arts and Sciences, American University, Washington D.C., USA

[2] District of Columbia Center for AIDS Research, Washington D.C., USA

[†]These authors contributed equally to this work

*Author to whom correspondence should be addressed

Abstract

The maturation of HIV-1 virions is a crucial process in viral replication. Although T cells are a primary source of virus production, much of our understanding of virion maturation comes from studies using the HEK293T human embryonic kidney cell line. Notably, there is a lack of comparative analyses between T cells and HEK293T cells in terms of virion maturation efficiency in existing literature. We previously developed an advanced virion visualization system based on the FRET principle, enabling the effective distinction between immature and mature virions via fluorescence microscopy. In this study, we utilized pseudotyped, single-round infectious viruses tagged with FRET labels (HIV-1 Gag-iFRETΔEnv) derived from Jurkat (a human T lymphocyte cell line) and HEK293T cells to evaluate their virion maturation rates. HEK293T-derived virions demonstrated a maturity rate of 81.79%, consistent with other studies and our previous findings. However, virions originating from Jurkat cells demonstrated a significantly reduced maturation rate of 68.67% ($p < 0.0001$). Correspondingly, viruses produced from Jurkat cells exhibited significantly reduced infectivity compared to those derived from HEK293T cells, with the relative infectivity measured at 65.3%. This finding is consistent with the observed relative maturation rate of viruses produced by Jurkat cells. These findings suggest that initiation of virion maturation directly correlates with viral infectivity. Our observation highlights the dynamic nature of virus-host interactions and their implications for virion production and infectivity.

Keywords:

Human Immunodeficiency Virus type I (HIV-1), Forster Resonance Energy Transfer (FRET), Virion Maturation, Comparative Viral Analysis, Fluorescent Microscopic Imaging,

1. Introduction

Human Immunodeficiency Virus-1 (HIV-1) continues to pose a significant global health challenge. The advancement of combination antivirals has dramatically improved the management of HIV-1, targeting various stages of the virus lifecycle, including entry, reverse transcription, integration, and protease activity [1-6]. Recently, the development of capsid inhibitors has emerged as a promising strategy for long-acting antiviral treatments against HIV-1 [7-12]. These novel inhibitors, targeting critical steps in both the early and late stages of the virus lifecycle, notably disrupt the formation of infectious particles. This innovation underscores the need for a comprehensive understanding of the virion maturation process, a key phase in the HIV-1 life cycle where non-infectious particles are transformed into infectious virions. Our previous research developed a unique tool for detecting virus maturation utilizing a fluorescence resonance energy transfer (FRET)-based technique [13]. This approach enables the semi-automatic evaluation of virion maturation through fluorescent microscopy, effectively minimizing human bias. It offers crucial insights into the structural changes that are vital for virus infectivity. Building upon this, our current study explores virion maturation in different cellular environments. Although T cells are recognized as the primary source for HIV-1 replication [14-20], most existing research assessing viral maturation predominantly utilizes the HEK293T human embryonic kidney cell line [21-24]. Utilizing the FRET-based system, we generated infectious FRET-labeled viruses in both HEK293T and Jurkat cells, an immortal human T-cell leukemia cell line. Surprisingly, we observed that viruses produced by Jurkat cells exhibited a significantly lower maturation efficiency (approximately 69%) compared to those from HEK293T cells (approximately 82%). In alignment with the observed differences in maturation rates, the infectivity of

viruses from Jurkat cells was approximately half that observed in viruses from HEK293T cells. Given that CD4+ T cells are the principal producers of HIV-1, these cells have evolved multiple antiretroviral mechanisms. For example, the HIV-1 Viral Infectivity Factor (Vif) is a crucial accessory molecule for HIV-1 replication in vivo. However, it is not necessary for HEK293T cells, as these kidney-derived cells do not express the potent antiviral host factor APOBEC3G [13, 25, 26]. It is highly plausible that kidney cells, having not been exposed to lentiviruses throughout evolutionary history, exhibit greater susceptibility to these viruses compared to T cells, which have been concurrently evolving to resist viral infections. This study is at the forefront of comparing virion maturation and infectivity among cell lines from different origins, highlighting a novel approach in this field of HIV-1 research.

2. Materials and Methods

2.1 Plasmid DNA Construction

The plasmid DNA utilized for HIV-1 Gag-iFRET labeling virus production incorporates an efficient intramolecular FRET pair, ECFPΔC11 and cp173Venus [27]. These genes are positioned between the MA and CA regions of the HIV-1 Gag protein based on the HIV-1 Gag-iGFP construct [28]. The FRET pair genes, along with the junction with the MA and CA regions, are flanked by HIV-1 protease cleavage sites (SQNYPIVQ). This design enables the HIV-1 Protease to specifically cleave at these sites, resulting in a modification of the FRET signal during the maturation of the virion. Additional details are provided in our previous publication [13].

2.2 Virus Production and Cell Culture

90 HIV-1 Gag-iFRET plasmid DNA was transfected into HEK293T cells using a PEI
91 transfection method (Polysciences) and into Jurkat cells using Lipofectamine LTX
92 transfection reagent (Invitrogen). HEK293T and TZM-bl cells were cultured in
93 Dulbecco's Modified Eagle's Medium (Cytiva) supplemented with 10% Fetal Bovine
94 Serum (Gibco), 1% Penicillin-Streptomycin-Glutamine (Invitrogen), and 1%
95 GlutaMax (Gibco)(D10) at 37°C in a 5% CO2 environment. Suspended Jurkat cells
96 were cultured in RPMI 1640 media (Cytiva) with the same supplements (R10). To
97 produce FRET-labelled virions, HEK293T cells (7.0×10^6 cells/10 cm dish) and
98 Jurkat cells (10×10^6 cells/10 cm dish) were co-transfected with pHIV-1 Gag-
99 iFRETΔEnv or iFRETΔProΔEnv, along with the parental plasmids pNL4-3ΔEnv or
100 pNL43ΔProΔEnv, and the pSVIII-92HT593.1 dual-tropic HIV-1 Env expression
101 plasmid, kindly provided by Dr. Viviana Simon at Mount Sinai, using a transfection
102 ratio of 1:10:2.5. The culture medium was replaced with fresh D10 medium after 3.5
103 hours for PEI transfection. Virus-containing supernatants were collected 48 hours
104 post-transfection. The supernatants were then filtered through a 0.45 μm sterile
105 polyvinylidene difluoride (PVDF, Millipore) membrane and concentrated up to 10-fold
106 using Lenti-X Concentrator (TaKaRa). The virus pellet was resuspended in 100 μL of
107 Phosphate Buffered Saline (PBS) without phenol red (Cytiva).

108

109 2.3 FRET-Based Virion Visualization

110 To visualize HIV-1 Gag-iFRETΔEnv/iFRETΔProΔEnv labeled virions, dilute the
111 concentrated virus supernatant 800-fold in 0.22 μm PVDF-filtered Hank's Balanced
112 Salt Solution (HBSS) without Phenol Red (Cytiva) and load 350 μL onto a glass-
113 bottomed 8-chamber slide (ibidi). The slide was then incubated overnight at 4°C.

114 Single-virion images were captured using an A1R MP+ Multiphoton Confocal
115 Microscope (Nikon). Two sets of 21 images were automatically acquired for each
116 sample under optimal focus conditions. The first set employed a 457.9 nm laser for
117 CFP excitation, capturing emissions through 482 nm/35 nm and 540 nm/30 nm filter
118 cubes for CFP and YFP signals, respectively (FRET images). The second set used a
119 514.5 nm laser for Venus excitation, with emissions read through a 540 nm/30 nm
120 filter cube to detect the YFP signal. The maturation status was quantified as FRET
121 efficiency relative to signals detected in HIV-1 Gag-iFRETΔ1ProΔEnv labeled virions.
122 Images were captured in RAW ND2 format and converted to TIFF files using Fiji, an
123 image processing package based on ImageJ2. Binary images, generated based on
124 the YFP signal, provided XY coordinates for each particle. Using these coordinates,
125 the FRET signal intensity of each virion was extracted from the raw data, and the
126 FRET ratio (YFP/CFP) was calculated for each particle. Histograms displaying the
127 distribution of FRET ratio values were generated, with 100 bins division, and kernel
128 density estimation curves were plotted alongside. The proportion of the total kernel
129 density estimation area overlapping with the HIV-1 Gag-iFRETΔProΔEnv area was
130 used to determine the proportion of immature virions. Image data analysis and
131 subsequent calculations of mature and immature virion proportions were performed
132 using an updated in-house MATLAB program [13].

133

134 2.4 Infectivity Assays

135 Viral titers were determined using the HIV-1 Gag p24 DuoSet ELISA (R&D Systems).
136 After seeding TZM-bl cells at 1×10^4 in flat-bottom 96-well plates (CELLTREAT),
137 they were exposed to an equivalent amount of virus (5 ng of HIV-1 p24 total) in the

following day. The cells were incubated at 37°C for 48 hours in a CO^2 incubator. Subsequently, luciferase activity in the infected cells was measured with the Luciferase Assay System (Promega) using a Molecular Devices SpectraMax Microplate Reader.

2.5 Statistical Analysis

Data were analyzed using standard statistical methods. The significance of differences in virion maturation and infectivity between the two cell types was determined using the Mann-Whitney U test and an unpaired *t*-test with Welch's correction, respectively, with a *p*-value of less than 0.05 considered statistically significant.

3. Results

3.1 Virion Maturation Efficiency in Different Producer Cells

In this study, we quantified the proportion of mature and immature virions in FRET-labeled viruses produced by HEK293T (kidney) and Jurkat (T-cell leukemia) cell lines. In each sample, we captured a total of 21 images, from which we created binary images based on the emitted and excited images of YFP (Fig. 1A). We then calculated the FRET ratio for each virion by dividing the intensity of YFP (the FRET acceptor) by the total CFP intensity, which serves as the FRET donor. After calculating the FRET ratio for each virion, based on the extracted signal intensities of the FRET donor and acceptor, we applied kernel density estimation to the histograms of FRET efficiencies. The area where the HIV-1 Gag-iFRETΔEnv curve

161 overlapped with the HIV-1 Gag-iFRETΔProΔEnv curve was identified as the
162 proportion of immature virions, as per our established methodology (Fig. 1B) [13]. In
163 our analysis, we examined 14,021 and 22,779 particles, as well as 20,457 and
164 23,181 particles of HIV-1 Gag-iFRETΔEnv and HIV-1 Gag-iFRETΔProΔEnv labeled
165 virions produced by HEK293T and Jurkat cells, respectively, across three
166 independent experiments. The mature virion proportion in the HIV-1 Gag-iFRETΔEnv
167 population from HEK293T cells was 81.79% ± 0.06 (Fig. 1C), consistent with our
168 previous findings and electron microscopic counts reported in other studies [13, 21-
169 24]. In contrast, Jurkat cells produced mature virions at a lower rate of 68.67% ±
170 0.04 (Fig. 1C), which is significantly different from that of HEK293T cells (*p*-value <
171 0.0001). Furthermore, we quantified the Mean Fluorescent Intensity (MFI) of the YFP
172 signal in both mature and immature virions. The results confirmed that the average
173 incorporation of fluorescent proteins, indicated by the MFI of YFP (Fig. 1D), was
174 similar in both mature and immature virions from HEK293T and Jurkat cells
175 (26,691.31 ± 2,733.73 vs. 23,309.51 ± 766.93 in mature virions and 24,619.37 ±
176 2,857.71 vs. 24,536.10 ± 2,046.71 in immature virions, respectively, and 24,619.37 ±
177 2,857.71 vs. 24,536.10 ± 2,036.70 in ΔPro). These findings indicate that the number
178 of incorporated fluorescent proteins is comparable, ensuring that the FRET energy
179 transfer efficiency is neither under nor overestimated in virions produced by either
180 HEK293T or Jurkat cells.

181

182 3.2 Virus Infectivity in Different Producer Cells

183 To further examine the characteristic differences between viruses produced by
184 HEK293T and Jurkat cells, we performed a single-round infection assay using TZM-

185 bl cells to assess the infectivity of FRET-labeled viruses originating from these cell
186 lines. The infectivity of viruses from Jurkat cells was significantly lower compared to
187 those from HEK293T cells, measured at 65.3% ± 5.6 (Fig. 2). This discrepancy is
188 consistent with the observed differences in the maturation rates of viruses produced
189 by Jurkat cells. (Fig. 1).

190

191 **4.1 Discussion**

192 The findings of this study provide groundbreaking insights into the maturation
193 process of HIV-1 virions and their impact on viral infectivity, challenging several
194 established concepts in the field. Our utilization of an advanced FRET-based
195 visualization system has allowed for a detailed comparative analysis of virion
196 maturation in two distinct cellular environments: HEK293T and Jurkat cell lines. One
197 of the most notable findings of our study is that virus maturation and subsequent
198 infectivity in T cell lines, which are derived from the natural targets for HIV-1, are
199 lower compared to kidney-derived cell lines. HEK293T cells exhibited a reduced rate
200 of immature virions (18.21%), whereas virions derived from Jurkat cells displayed a
201 higher rate of immaturity (31.33%), correlating with its respective infectivity (65.3% ±
202 5.6 for Jurkat cell-derived virions compared to the infectivity observed in virions from
203 HEK293T cells). Recent studies have provided deeper insights into the role of
204 inositol hexakisphosphate (IP6) in HIV-1 capsid assembly, which is a critical factor in
205 virus infectivity [29]. These studies reveal that the immature Gag lattice of HIV-1
206 virions enriches IP6, facilitating capsid maturation. This process is characterized by
207 proteolysis of the Gag polyprotein by the viral protease, which induces vital
208 conformational changes in the capsid protein (CA). These changes led to the

209 formation of a conical, cone-shaped mature capsid consisting of over 1,000 CA
210 copies and forming approximately 200 hexamers and 12 pentamers, collectively
211 known as capsomers. Sowd et al. showed that IP6-depleted T-cell lines produce
212 virion particles with incompletely cleaved Gag proteins [30]. This study indicated that
213 virions from IP6-deficient cells exhibited lower quantities of mature MA and CA
214 cleavage products and higher proportions of MA-CA-SP1/MA-CA cleavage
215 intermediates than virions from wild-type cells. In the context of our FRET-based
216 assay, which specifically detects cleavage of the Gag polyprotein between MA-CA,
217 our FRET detection system can potentially monitor the IP6-dependent efficiency of
218 Gag polyprotein cleavage. Furthermore, they characterized virus particle morphology
219 using electron microscopy and calculated that mature particles in another T-cell
220 leukemia cell line, MT-4 cells, comprised 62% of the total virions, which aligns with
221 the results from our FRET detection system in Jurkat cells (Fig. 1B [II], and 1C).
222 Given that the majority of inositol synthesis in humans occurs in kidney tissue [31], it
223 is reasonable to infer that HEK293T cells would exhibit abundant IP6 expression.
224 This is likely to contribute to enhanced virion maturation efficiency.
225 Another study employing a similar concept of FRET-based assay with different FRET
226 pair proteins revealed that the activation of HIV-1 viral protease occurs during
227 assembly and budding before the release of particles in HEK293T cells [32]. The
228 early maturation observed in HEK293T cells could lead to an increase in progeny
229 virion maturation. This effect likely accounts for the elevated maturation ratio
230 observed in HEK293T cells in our study (Fig. 1). This early maturation could also
231 result in enhanced viral infectivity compared to virions originating from Jurkat cells
232 (Fig. 2). Mathematical modeling suggests that transport of the pre-integration
233 complex into the nucleus, along with DNA integration and reverse transcription, is

234 one of the major factors that significantly influences HIV-1 replication [33]. The
235 formation of a conical core is essential for both steps of reverse transcription and the
236 subsequent transport of viral DNA into the nucleus for integration into the host
237 genome [34, 35]. Consequently, the formation of an infectious conical core following
238 Gag polyprotein cleavage is a critical determinant of viral infectivity. This suggests
239 that viruses originating from T cell lines might be less efficient at forming appropriate
240 conical cores, which, paradoxically, may reduce their infectivity.
241 On another note, it is crucial to recognize that the recruitment of viral envelope (Env)
242 glycoproteins onto progeny virions plays a pivotal role in achieving virus infectivity.
243 The MA domain of the Gag polyprotein not only directs the Gag to the plasma
244 membrane but also facilitates the incorporation of the Env protein [36]. The
245 trimerization of the MA domain is critically important for the efficient incorporation of
246 Env proteins [37]. The Gag precursor, which encompasses the CA domain, is
247 instrumental in facilitating the trimerization of the MA domain [38]. Another study has
248 suggested that IP6 plays a crucial role in facilitating the assembly of the immature
249 HIV-1 Gag lattice [39]. Consequently, the elevated expression of IP6 in HEK293T
250 cells might enhance the assembly of Gag precursors at the budding site prior to
251 virion release, potentially initiating the trimerization of the MA domain. This, in turn,
252 could enhance the efficient incorporation of Env proteins into progeny virions.
253 Several accessory molecules, such as Vif, are not required to produce infectious
254 viruses from HEK293T cells [13, 25, 26]. This is due to the absence of antiviral host
255 factors in HEK293T cells that would normally be counteracted by viral accessory
256 proteins. This discrepancy may hint at the heightened susceptibility of kidney cells to
257 retrovirus infection, potentially attributable to their lack of prior exposure to these viral
258 components. Thus, the environment in HEK293T cells is optimized not only by the

absence of antiviral host protein expression but also by the enrichment of host cofactors, which collectively contribute to increased virus infectivity.

Our research addresses a critical gap in the existing literature by presenting a comparative analysis of the efficiency of Gag polyprotein cleavage in virions produced by kidney cells (HEK293T) and T cells (Jurkat). This comparison is vital, considering T cells are the primary source of HIV-1 replication *in vivo*. The observed differences in maturation efficiencies and infectivity rates between HEK293T and Jurkat cells highlight the importance of considering the cellular context in HIV-1 biology and pathogenesis studies. Furthermore, our findings have significant implications for the evaluation of antiviral effects, particularly in the context of long-acting treatments with maturation and capsid inhibitors. These inhibitors target various stages of virus infection, including viral budding and virion maturation [36, 40, 41]. The substantial disparities in viral maturation rates between T-cells and HEK293T cells, the latter of which is a standard cellular resource for *in-vitro* virus production, suggest that relying solely on HEK293T cells could lead to misleading assessments of antiviral efficacy. Therefore, our study indicates the necessity of including T-cell-based assessments to more accurately determine the antiviral efficacy of maturation and capsid inhibitors in virus maturation.

In conclusion, the results of our study not only enhance our understanding of HIV-1 pathogenesis but also emphasize the complexity of the virus life cycle. The unique insights gained into the relationship between virion maturation and infectivity open new pathways for future research, potentially leading to novel therapeutic approaches in the fight against HIV-1.

Author's contributions

284 TI conceptualized and designed the study. Experiments were carried out by JC, AM,
285 SG, HT, LMB, CA, and TI. The development of the in-house MATLAB script for
286 automated image data analysis was a collaborative effort between KN and TI. Data
287 analysis was conducted by KN, SG, and TI. The manuscript was written by TI. TI
288 provides financial support for the research. All authors have made substantial
289 contributions to the work and have given their approval for the final version of the
290 article to be published.

291

292 **Funding**

293 This study is partially supported by a research start-up fund from American
294 University (Grant Number: 75316 to TI). Additional funding was provided by the
295 National Institutes of Health, specifically through a grant from the National Institute of
296 Allergy and Infectious Diseases (Grant Number: 7R15AI172610-02 to TI).

297

298 **Acknowledgments**

299 We extend our thanks to Dr. Viviana Simon at Mount Sinai for generously providing
300 the pSVIII-92HT593.1 plasmid DNA.

301

302 **Figure Legend**

303 **Figure 1. Quantitative Analysis of Mature Virions from HEK293T and Jurkat**
304 **Cells.**

305 (A) Representative FRET-labeled HIV-1 Gag-iFRETΔEnv virion images from Jurkat
306 cells displayed in a single field. The left panel shows an image captured through the
307 YFP excitation (515 nm) and emission (540 nm) channels (YFP channel). The
308 second image shows the binary image, derived from the YFP channel, identifying
309 virus particle locations as regions of interest (ROI). The third and fourth images are
310 captured using CFP (FRET donor) excitation (454 nm), with CFP emission (483 nm,
311 third) and YFP emission (540 nm, fourth) channels. The right panel shows the FRET
312 efficiency ratio view, computationally constructed from FRET donor (CFP
313 excitation/CFP emission) and acceptor (CFP excitation/YFP emission) images. The
314 color spectrum indicates FRET signal strength, with high FRET appearing in red
315 (yellow arrows) and decreasing FRET shifting toward blue (white arrows). (B) Kernel
316 Density Estimation Curves of FRET Intensity in HIV-1 Gag-iFRETΔEnv Virions
317 Produced by HEK293T and Jurkat Cells. The curves depict the distribution
318 histograms of FRET intensity for virions labeled with HIV-1 Gag-iFRETΔEnv from (I)
319 HEK293T and (II) Jurkat cells. The x-axis represents the range of FRET intensity.
320 The y-axis shows the adjusted density of curves for both HIV-1 Gag-iFRETΔEnv and
321 HIV-1 Gag-iFRETΔProΔEnv virions. The area under the curve for HIV-1 Gag-
322 iFRETΔEnv overlapping with that of HIV-1 Gag-iFRETΔProΔEnv is calculated and
323 considered indicative of the proportion of immature virions within the total population
324 of HIV-1 Gag-iFRETΔEnv virions. (C) Scatter Plot of Mature Virion Quantification
325 displays the median percentage of mature virions across 21 images derived from
326 three independent experiments, culminating in a total of 63 data points. Statistical
327 significance was assessed using the Mann-Whitney U test. (D) Comparison of Mean
328 Fluorescent Intensity (MFI) of YFP Signals in Mature and Immature HIV-1 Gag-
329 iFRETΔEnv labeling Virions. The levels of fluorescent protein incorporation, as

330 indicated by the YFP signal, were not significantly different between mature and
331 immature virions in either the wild-type or ΔPro viruses. The error bars represent the
332 standard error from three independent experiments. Statistical significance was
333 assessed using the Wilcoxon matched-pairs signed rank test.

334

335 **Figure 2. Comparing Virus Infectivity Between HEK293T and Jurkat Cells**.

336 Single-round infectivity assays using TZM-bl cells were performed to evaluate the
337 differences in virus infectivity produced by HEK293T and Jurkat cells. The bar plot
338 illustrates the relative infectivity of the FRET-labeled virus produced by Jurkat cells in
339 comparison to its infectivity when produced by HEK293T cells. Error bars represent
340 the standard deviation from three independent experiments. Statistical significance
341 was determined using an unpaired *t*-test with Welch's correction.

342

343 **References**

344 1. Ghosh, A. K., Four decades of continuing innovations in the development of
345 antiretroviral therapy for HIV/AIDS: Progress to date and future challenges. *Glob*
346 *Health Med* **2023,** 5, (4), 194-198.
347 2. Landovitz, R. J.; Scott, H.; Deeks, S. G., Prevention, treatment and cure of HIV
348 infection. *Nat Rev Microbiol* **2023,** 21, (10), 657-670.
349 3. Arts, E. J.; Hazuda, D. J., HIV-1 antiretroviral drug therapy. *Cold Spring Harb*
350 *Perspect Med* **2012,** 2, (4), a007161.
351 4. Magden, J.; Kaariainen, L.; Ahola, T., Inhibitors of virus replication: recent
352 developments and prospects. *Appl Microbiol Biotechnol* **2005,** 66, (6), 612-21.
353 5. Adamson, C. S.; Freed, E. O., Novel approaches to inhibiting HIV-1 replication.
354 *Antiviral Res* **2010,** 85, (1), 119-41.
355 6. Wiebe, L. I.; Knaus, E. E., Concepts for the design of anti-HIV nucleoside prodrugs
356 for treating cephalic HIV infection. *Adv Drug Deliv Rev* **1999,** 39, (1-3), 63-80.
357 7. Thenin-Houssier, S.; Valente, S. T., HIV-1 Capsid Inhibitors as Antiretroviral Agents.
358 *Curr HIV Res* **2016,** 14, (3), 270-82.
359 8. Yant, S. R.; Mulato, A.; Hansen, D.; Tse, W. C.; Niedziela-Majka, A.; Zhang, J. R.;
360 Stepan, G. J.; Jin, D.; Wong, M. H.; Perreira, J. M.; Singer, E.; Papalia, G. A.; Hu, E.
361 Y.; Zheng, J.; Lu, B.; Schroeder, S. D.; Chou, K.; Ahmadyar, S.; Liclican, A.; Yu, H.;
362 Novikov, N.; Paoli, E.; Gonik, D.; Ram, R. R.; Hung, M.; McDougall, W. M.; Brass,
363 A. L.; Sundquist, W. I.; Cihlar, T.; Link, J. O., A highly potent long-acting small-
364 molecule HIV-1 capsid inhibitor with efficacy in a humanized mouse model. *Nat Med*
365 **2019,** 25, (9), 1377-1384.

366 9. Singh, K.; Gallazzi, F.; Hill, K. J.; Burke, D. H.; Lange, M. J.; Quinn, T. P.; Neogi, U.;
367 Sonnerborg, A., GS-CA Compounds: First-In-Class HIV-1 Capsid Inhibitors Covering
368 Multiple Grounds. *Front Microbiol* **2019,** 10, 1227.
369 10. Sun, L.; Zhang, X.; Xu, S.; Huang, T.; Song, S.; Cherukupalli, S.; Zhan, P.; Liu, X.,
370 An insight on medicinal aspects of novel HIV-1 capsid protein inhibitors. *Eur J Med*
371 *Chem* **2021,** 217, 113380.
372 11. Flexner, C.; Owen, A.; Siccardi, M.; Swindells, S., Long-acting drugs and
373 formulations for the treatment and prevention of HIV infection. *Int J Antimicrob*
374 *Agents* **2021,** 57, (1), 106220.
375 12. Gillis, E. P.; Parcella, K.; Bowsher, M.; Cook, J. H.; Iwuagwu, C.; Naidu, B. N.; Patel,
376 M.; Peese, K.; Huang, H.; Valera, L.; Wang, C.; Kieltyka, K.; Parker, D. D.;
377 Simmermacher, J.; Arnoult, E.; Nolte, R. T.; Wang, L.; Bender, J. A.; Frennesson, D.
378 B.; Saulnier, M.; Wang, A. X.; Meanwell, N. A.; Belema, M.; Hanumegowda, U.;
379 Jenkins, S.; Krystal, M.; Kadow, J. F.; Cockett, M.; Fridell, R., Potent Long-Acting
380 Inhibitors Targeting the HIV-1 Capsid Based on a Versatile Quinazolin-4-one
381 Scaffold. *J Med Chem* **2023,** 66, (3), 1941-1954.
382 13. Sarca, A. D.; Sardo, L.; Fukuda, H.; Matsui, H.; Shirakawa, K.; Horikawa, K.;
383 Takaori-Kondo, A.; Izumi, T., FRET-Based Detection and Quantification of HIV-1
384 Virion Maturation. *Front Microbiol* **2021,** 12, 647452.
385 14. Chen, B., Molecular Mechanism of HIV-1 Entry. *Trends Microbiol* **2019,** 27, (10),
386 878-891.
387 15. Pan, X.; Baldauf, H. M.; Keppler, O. T.; Fackler, O. T., Restrictions to HIV-1
388 replication in resting CD4+ T lymphocytes. *Cell Res* **2013,** 23, (7), 876-85.
389 16. Banga, R.; Procopio, F. A.; Noto, A.; Pollakis, G.; Cavassini, M.; Ohmiti, K.;
390 Corpataux, J. M.; de Leval, L.; Pantaleo, G.; Perreau, M., PD-1(+) and follicular

391 helper T cells are responsible for persistent HIV-1 transcription in treated aviremic
392 individuals. *Nat Med* **2016,** 22, (7), 754-61.
393 17. Berg, R. K.; Rahbek, S. H.; Kofod-Olsen, E.; Holm, C. K.; Melchjorsen, J.; Jensen, D.
394 G.; Hansen, A. L.; Jorgensen, L. B.; Ostergaard, L.; Tolstrup, M.; Larsen, C. S.;
395 Paludan, S. R.; Jakobsen, M. R.; Mogensen, T. H., T cells detect intracellular DNA
396 but fail to induce type I IFN responses: implications for restriction of HIV replication.
397 *PLoS One* **2014,** 9, (1), e84513.
398 18. Jones, R. B.; Ndhlovu, L. C.; Barbour, J. D.; Sheth, P. M.; Jha, A. R.; Long, B. R.;
399 Wong, J. C.; Satkunarajah, M.; Schweneker, M.; Chapman, J. M.; Gyenes, G.; Vali,
400 B.; Hyrcza, M. D.; Yue, F. Y.; Kovacs, C.; Sassi, A.; Loutfy, M.; Halpenny, R.; Persad,
401 D.; Spotts, G.; Hecht, F. M.; Chun, T. W.; McCune, J. M.; Kaul, R.; Rini, J. M.;
402 Nixon, D. F.; Ostrowski, M. A., Tim-3 expression defines a novel population of
403 dysfunctional T cells with highly elevated frequencies in progressive HIV-1 infection.
404 *J Exp Med* **2008,** 205, (12), 2763-79.
405 19. Zhang, Z.; Schuler, T.; Zupancic, M.; Wietgrefe, S.; Staskus, K. A.; Reimann, K. A.;
406 Reinhart, T. A.; Rogan, M.; Cavert, W.; Miller, C. J.; Veazey, R. S.; Notermans, D.;
407 Little, S.; Danner, S. A.; Richman, D. D.; Havlir, D.; Wong, J.; Jordan, H. L.;
408 Schacker, T. W.; Racz, P.; Tenner-Racz, K.; Letvin, N. L.; Wolinsky, S.; Haase, A. T.,
409 Sexual transmission and propagation of SIV and HIV in resting and activated CD4+ T
410 cells. *Science* **1999,** 286, (5443), 1353-7.
411 20. Groot, F.; van Capel, T. M.; Schuitemaker, J.; Berkhout, B.; de Jong, E. C.,
412 Differential susceptibility of naive, central memory and effector memory T cells to
413 dendritic cell-mediated HIV-1 transmission. *Retrovirology* **2006,** 3, 52.

414 21. Mattei, S.; Flemming, A.; Anders-Osswein, M.; Krausslich, H. G.; Briggs, J. A.;
415 Muller, B., RNA and Nucleocapsid Are Dispensable for Mature HIV-1 Capsid
416 Assembly. *J Virol* **2015,** 89, (19), 9739-47.
417 22. Keller, P. W.; Huang, R. K.; England, M. R.; Waki, K.; Cheng, N.; Heymann, J. B.;
418 Craven, R. C.; Freed, E. O.; Steven, A. C., A two-pronged structural analysis of
419 retroviral maturation indicates that core formation proceeds by a disassembly-
420 reassembly pathway rather than a displacive transition. *J Virol* **2013,** 87, (24), 13655-
421 64.
422 23. Fontana, J.; Jurado, K. A.; Cheng, N.; Ly, N. L.; Fuchs, J. R.; Gorelick, R. J.;
423 Engelman, A. N.; Steven, A. C., Distribution and Redistribution of HIV-1
424 Nucleocapsid Protein in Immature, Mature, and Integrase-Inhibited Virions: a Role
425 for Integrase in Maturation. *J Virol* **2015,** 89, (19), 9765-80.
426 24. Hanne, J.; Gottfert, F.; Schimer, J.; Anders-Osswein, M.; Konvalinka, J.; Engelhardt,
427 J.; Muller, B.; Hell, S. W.; Krausslich, H. G., Stimulated Emission Depletion
428 Nanoscopy Reveals Time-Course of Human Immunodeficiency Virus Proteolytic
429 Maturation. *ACS Nano* **2016,** 10, (9), 8215-22.
430 25. Sheehy, A. M.; Gaddis, N. C.; Choi, J. D.; Malim, M. H., Isolation of a human gene
431 that inhibits HIV-1 infection and is suppressed by the viral Vif protein. *Nature* **2002,**
432 418, (6898), 646-50.
433 26. Izumi, T.; Shirakawa, K.; Takaori-Kondo, A., Cytidine deaminases as a weapon
434 against retroviruses and a new target for antiviral therapy. *Mini Rev Med Chem* **2008,**
435 8, (3), 231-8.
436 27. Nagai, T.; Miyawaki, A., A high-throughput method for development of FRET-based
437 indicators for proteolysis. *Biochem Biophys Res Commun* **2004,** 319, (1), 72-7.

438 28. Hubner, W.; Chen, P.; Del Portillo, A.; Liu, Y.; Gordon, R. E.; Chen, B. K., Sequence
439 of human immunodeficiency virus type 1 (HIV-1) Gag localization and
440 oligomerization monitored with live confocal imaging of a replication-competent,
441 fluorescently tagged HIV-1. *J Virol* **2007,** 81, (22), 12596-607.
442 29. Renner, N.; Kleinpeter, A.; Mallery, D. L.; Albecka, A.; Rifat Faysal, K. M.; Bocking,
443 T.; Saiardi, A.; Freed, E. O.; James, L. C., HIV-1 is dependent on its immature lattice
444 to recruit IP6 for mature capsid assembly. *Nat Struct Mol Biol* **2023,** 30, (3), 370-382.
445 30. Sowd, G. A.; Aiken, C., Correction: Inositol phosphates promote HIV-1 assembly and
446 maturation to facilitate viral spread in human CD4+ T cells. *PLoS Pathog* **2021,** 17,
447 (3), e1009389.
448 31. Parthasarathy, L. K.; Seelan, R. S.; Tobias, C.; Casanova, M. F.; Parthasarathy, R. N.,
449 Mammalian inositol 3-phosphate synthase: its role in the biosynthesis of brain inositol
450 and its clinical use as a psychoactive agent. *Subcell Biochem* **2006,** 39, 293-314.
451 32. Tabler, C. O.; Wegman, S. J.; Chen, J.; Shroff, H.; Alhusaini, N.; Tilton, J. C., The
452 HIV-1 Viral Protease Is Activated during Assembly and Budding Prior to Particle
453 Release. *J Virol* **2022,** 96, (9), e0219821.
454 33. Shcherbatova, O.; Grebennikov, D.; Sazonov, I.; Meyerhans, A.; Bocharov, G.,
455 Modeling of the HIV-1 Life Cycle in Productively Infected Cells to Predict Novel
456 Therapeutic Targets. *Pathogens* **2020,** 9, (4).
457 34. Burdick, R. C.; Li, C.; Munshi, M.; Rawson, J. M. O.; Nagashima, K.; Hu, W. S.;
458 Pathak, V. K., HIV-1 uncoats in the nucleus near sites of integration. *Proc Natl Acad*
459 *Sci U S A* **2020,** 117, (10), 5486-5493.
460 35. Li, C.; Burdick, R. C.; Nagashima, K.; Hu, W. S.; Pathak, V. K., HIV-1 cores retain
461 their integrity until minutes before uncoating in the nucleus. *Proc Natl Acad Sci U S A*
462 **2021,** 118, (10).

463 36. Freed, E. O., HIV-1 assembly, release and maturation. *Nat Rev Microbiol* **2015,** 13,
464 (8), 484-96.
465 37. Tedbury, P. R.; Novikova, M.; Alfadhli, A.; Hikichi, Y.; Kagiampakis, I.;
466 KewalRamani, V. N.; Barklis, E.; Freed, E. O., HIV-1 Matrix Trimerization-Impaired
467 Mutants Are Rescued by Matrix Substitutions That Enhance Envelope Glycoprotein
468 Incorporation. *J Virol* **2019,** 94, (1).
469 38. Tang, C.; Loeliger, E.; Luncsford, P.; Kinde, I.; Beckett, D.; Summers, M. F., Entropic
470 switch regulates myristate exposure in the HIV-1 matrix protein. *Proc Natl Acad Sci*
471 *U S A* **2004,** 101, (2), 517-22.
472 39. Dick, R. A.; Zadrozny, K. K.; Xu, C.; Schur, F. K. M.; Lyddon, T. D.; Ricana, C. L.;
473 Wagner, J. M.; Perilla, J. R.; Ganser-Pornillos, B. K.; Johnson, M. C.; Pornillos, O.;
474 Vogt, V. M., Inositol phosphates are assembly co-factors for HIV-1. *Nature* **2018,** 560,
475 (7719), 509-512.
476 40. Wang, D.; Lu, W.; Li, F., Pharmacological intervention of HIV-1 maturation. *Acta*
477 *Pharm Sin B* **2015,** 5, (6), 493-9.
478 41. Kleinpeter, A. B.; Freed, E. O., HIV-1 Maturation: Lessons Learned from Inhibitors.
479 *Viruses* **2020,** 12, (9).

480

Figure 1

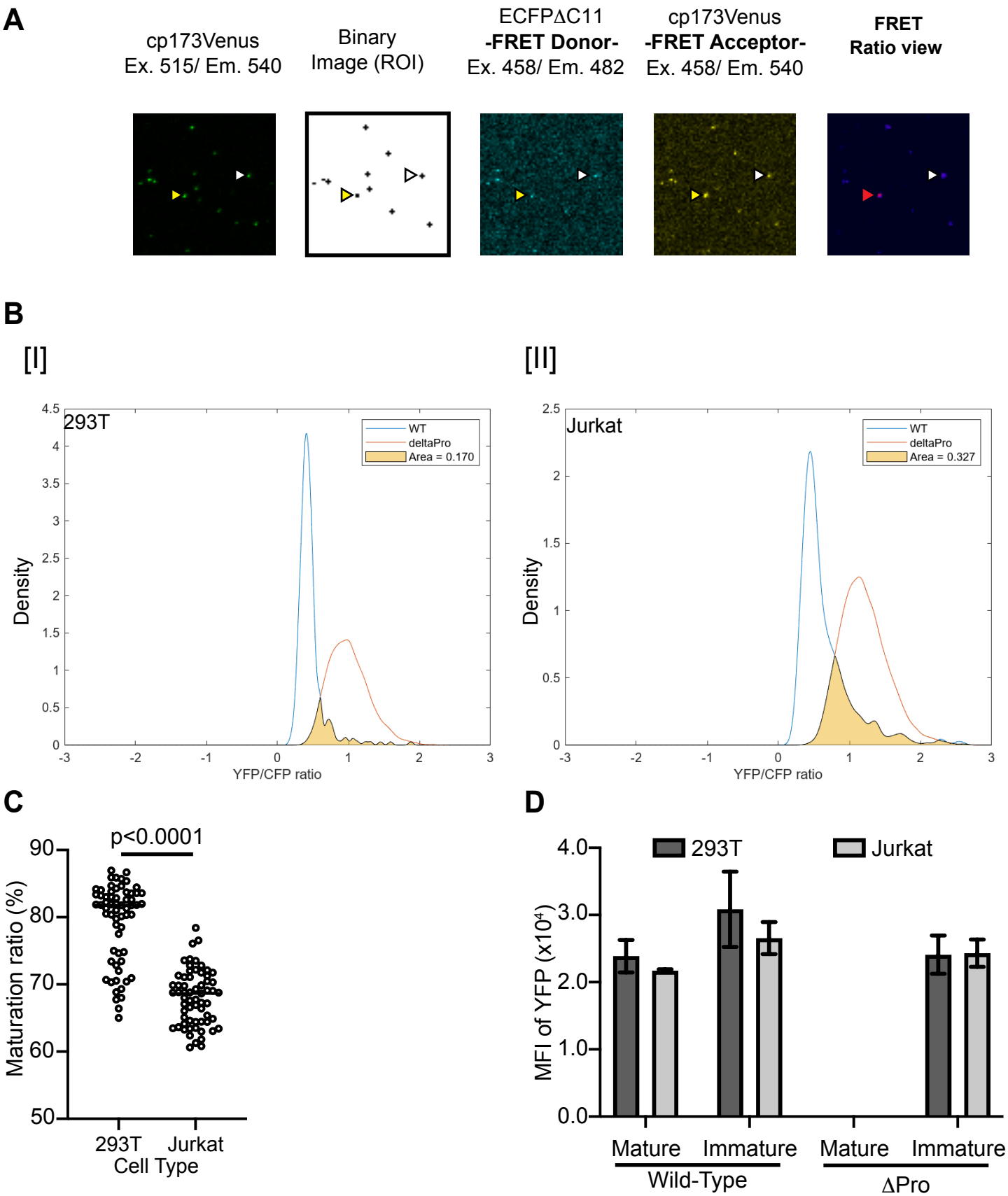
A
cp173Venus
Ex. 515/ Em. 540
Binary
Image (ROI)
ECFPΔC11
-FRET Donor-
Ex. 458/ Em. 482
cp173Venus
-FRET Acceptor-
Ex. 458/ Em. 540
FRET
Ratio view
B
[I]
293T
WT
deltaPro
Area = 0.170
Density
YFP/CFP ratio
[II]
Jurkat
WT
deltaPro
Area = 0.327
Density
YFP/CFP ratio
C
p<0.0001
Maturation ratio (%)
293T
Jurkat
Cell Type
D
293T
Jurkat
MFI of YFP (x10⁴)
Mature
Immature
Wild-Type
Mature
Immature
ΔPro

Figure 2

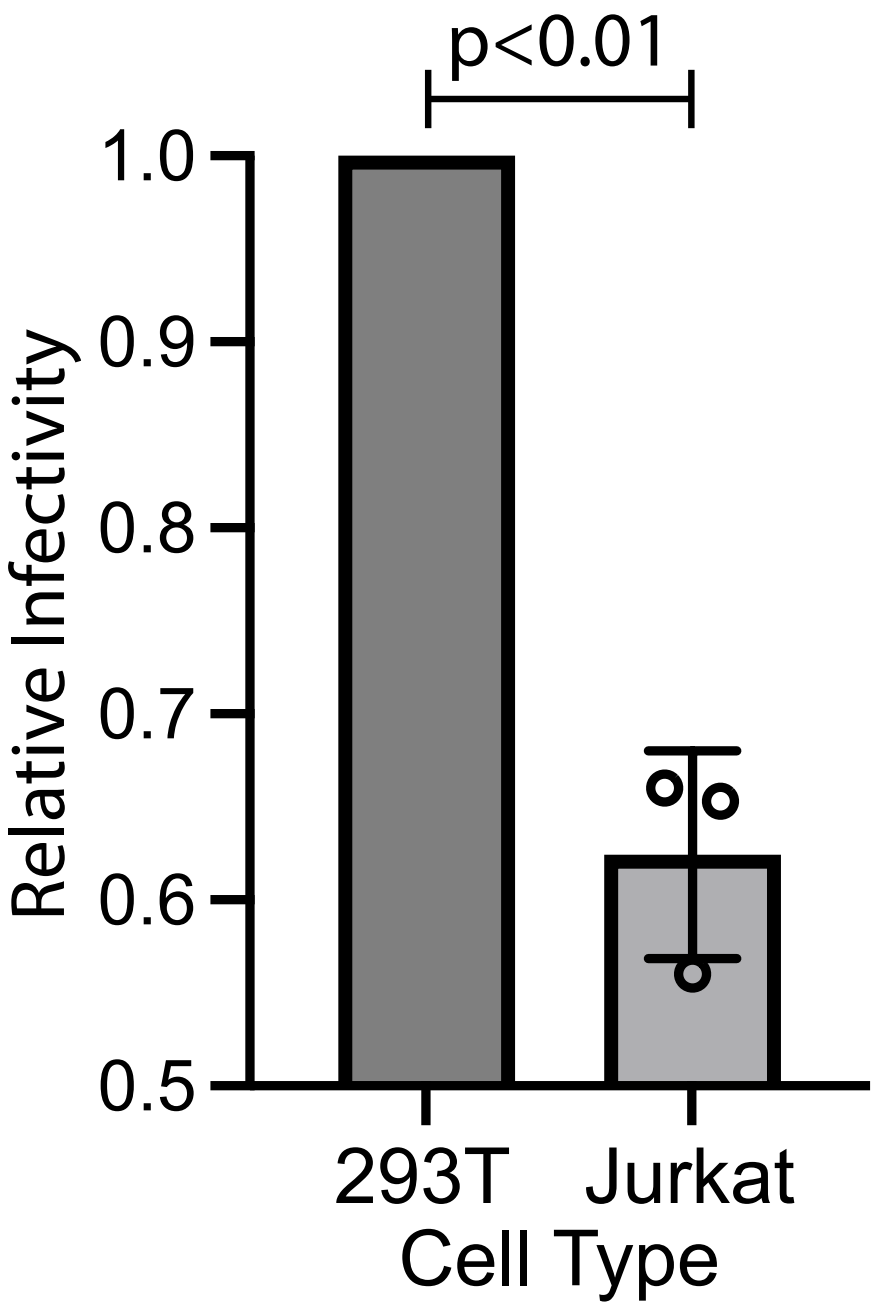
p<0.01
1.0
0.9
0.8
0.7
0.6
0.5
Relative Infectivity
293T
Jurkat
Cell Type